# Proton Release from the Histidine-Tetrad in the M2 Channel of the Influenza A Virus

Hao Dong,[†] Giacomo Fiorin,[†] William F. DeGrado,[‡] and Michael L. Klein*,[†]

[†]Institute for Computational Molecular Science, Temple University, 1900 North 12th Street, Philadelphia, Pennsylvania 19122-6078, United States

[‡]Department of Pharmaceutical Chemistry, University of California, San Francisco, 555 Mission Bay Boulevard South, San Francisco, California 94158-9001, United States

ABSTRACT: The activity of the M2 proton channel of the influenza A virus is controlled by pH. The tautomeric state and conformation of His37, a key residue in the M2 transmembrane four-helix bundle, controls the gating of the channel. Previously, we compared the energetics and dynamics of two alternative conformations of the doubly protonated state at neutral pH, namely, a 4-fold symmetric "histidine-box" and a 2-fold symmetric "dimer-of-dimers", and proposed a multiconfiguration model for this charge state. Here, we elaborate this model by further studying configurations of the His37 tetrad in the triply protonated state and its subsequent

deprotonation via quantum mechanics/molecular mechanics (QM/MM) molecular dynamics (MD) simulations, starting with the aforementioned configurations, to gain information about proton release in a viral membrane environment. Interestingly, the two configurations converge under acidic pH conditions. Protons can be transferred from one charged His37 to a neighboring water cluster at the C-terminal side of the channel when the Trp41 gate is open transiently. With limited backbone expansion, the free energy barrier for proton release to the viral interior at low pH is ∼6.5 kcal/mol in both models, which is much lower than at either neutral pH or for an isolated His37 cluster without a membrane environment. Our calculations also suggest that the M2 protein would seem to exclude the entrance of anions into the central channel through a special mechanism, due to the latter's potential inhibitory effect on proton conduction.
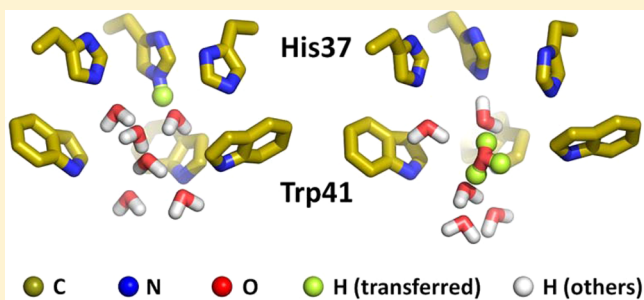
INTRODUCTION

Proton transfer is a ubiquitous phenomenon in chemical and biological systems. Interestingly, the trajectory of a proton in the lumen of the so-called M2 channel of the influenza A virus is an example from Biology. The M2 integral membrane protein is a tetramer assembled from four identical subunits, each with 97 residues.[1,2] As a prerequisite for release of genetic material to the cytoplasm, the interior of a viral particle must become acidified as a means to detect its own entrance in the endosome.[2] The M2 protein channel fulfills this acidification function by conducting protons through its membrane pore. The gating of this essential proton transport step in the infection cycle is controlled by pH.[3−5]

Among the pore-lining residues, His37 and Trp41 were identified as the most important residues in the proton transfer through the M2 channel. The proton selective conductance in M2 is achieved by the presence of the His37 cluster: substitution of His37 with residues such as Gly or Ala induces a nonselective channel, indicating a mechanistic role of His37 in proton relay.[6,7] Each of the four His37 may have two tautomeric forms at neutral conditions. A transfer cycle was proposed where a tautomerization of the His37 side chain occurs between the acceptance of a proton from the viral exterior and the release of a proton to the viral interior, to

reestablish in full the original configuration for the next cycle. On replacing the imidazole ring of the His37 side chain with a 4-thiazolyl group, which has the Nε1 as the only proton acceptor with pKa ∼2.5, this mutant shows inward proton flux resembling the wild type, thus demonstrating that tautomerization is not necessarily required for proton transport.[8] However, rotation of the imidazole ring during proton translocation cannot be ruled out. Besides the functional role in proton selectivity, His37 is associated with channel activation: binding of a third proton to the His37 cluster under acidic conditions triggers a detectable proton flux, with a peak conductance rate of 10^4 protons per second.[3,9] Trp41, on the other hand, serves as the channel gate.[10,11] Substitution of Trp41 with smaller residues, like Gly, Ala and Phe, induces higher proton conductivity compared to the wild-type channel.[10]

Despite the relatively small size of the M2 protein, and several high-resolution structures being available, the mechanism of proton conduction through the channel is not completely understood (Figure 1A).[12] Previously, we studied the addition of a proton to the His37 cluster from the extraviral
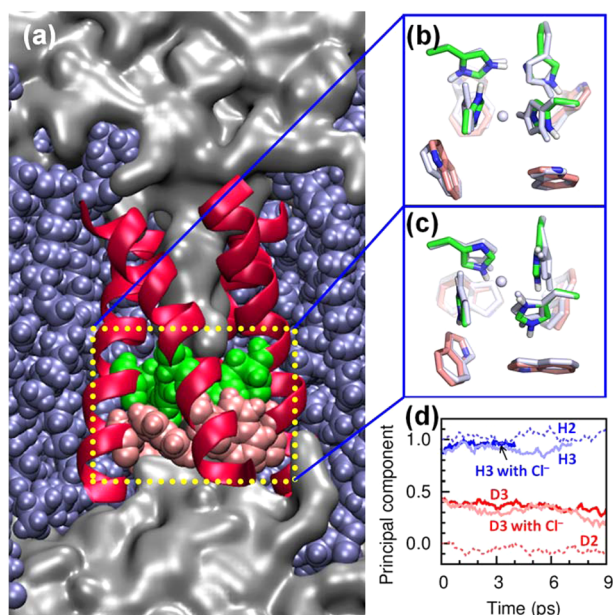
Figure 1. M2 channel and its two configurations of the His37···Trp41 quartet at low pH. (a) Shown is the TM domain of M2 protein imbedded in a fully hydrated lipid bilayer. The backbone is shown as red helices. His37 and Trp41 residues and lipids are colored in green, pink, and ice blue, respectively, as space filling spheres. Waters are shown in gray surface. The D-model (b) and the H-model (c) of the quartet. System with the absence of Cl⁻ ion are shown in stick mode with the same color code as in (a), and the system with Cl⁻ ion are shown in white stick. (d) The principal components of the quartet, λ, in different systems as a function of time; data for the 2+ state are shown for comparison.

side,[13] and compared the energetics and dynamics of two configurations of the doubly protonated state at neutral pH—a 4-fold symmetric "histidine-box" and a 2-fold symmetric "dimer-of-dimers"—and proposed a multiconfiguration model where these configurations are in moderately fast equilibrium.[14] Here, we focus our analysis on the configuration of the His37···Trp41 cluster in the triply protonated state, and its subsequent deprotonation.

Herein, quantum mechanics/molecular mechanics (QM/MM) molecular dynamics (MD) simulations reveal insights into the function and mechanism of this protein. Specifically, molecular simulations complemented by crystallographic and NMR (nuclear magnetic resonance) determined structural data, as well as physiological measurements provide mechanistic clues in understanding this rate-limiting step of proton conduction in M2, especially the proton trajectory during the translocation "reaction". The present study elaborates our previous computational works, and explores the free energy profile with the explicit presence of the complete transmembrane domain of the protein as well as a fully hydrated membrane environment. Moreover, to explore the effect of the proton filter and the channel gate, the entire His37···Trp41 cluster and the nearby water clusters are treated within a quantum mechanical methodology.

In this manuscript, we document multiple calculations: first, we studied the structural integrity of the M2 protein with two models at low pH with QM/MM MD simulations. We find that the structures of the His37 cluster starting from both models converge at low pH, and are stable within the simulation time scale: both models appear ready for the subsequent proton

release toward the intraviral side. Then, we calculated potentials of mean force (PMFs) of the deprotonation by constrained QM/MM MD simulations: the PMFs of both models have barriers ~6.5 kcal/mol. Compared to previous simulation studies, the local electrostatic environment of the hydrated membrane significantly lowers the energy cost. Finally, we explored the possible role of a Cl⁻ anion in the pore at low pH, which was found to stabilize the highly charged 3+ histidine cluster, but also to impede proton release by stabilizing the hydronium species within the channel pore.

COMPUTATIONAL DETAILS

For clarity, we named the "dimer-of-dimers" configuration at the 2+ state (with 2 of 4 His37 side chains charged) at neutral pH as the "D2-model", and the subsequent 3+ state obtained by adding a third proton as the "D3-model" (Figure 1B). Correspondingly, the "histidine-box" at 2+ state and the subsequent 3+ state structures are designated as the "H2-" and "H3-models" (Figure 1C), respectively.

Classical MD Simulations. The 1.65 Å resolution X-ray structure (pdb entry: 3LBW, residues 25−46) was used as the initial structure.[15] Two and three of the four His37 residues were initialized to be charged in the 2+ and 3+ states, respectively. The protein was then embedded in a previously equilibrated 80 × 80 Å² lipid bilayer containing 171 1-palmytoyl-2-oleoyl-*sn*-glycero-3-phosphatidylcholine (POPC) molecules, hydrated by 10,031 water molecules. Potassium and chloride ions were added to neutralize the system, and to provide a solution buffer with ionic concentration of 150 mM.

Periodic boundary conditions were applied, and long-range electrostatic interactions were treated with the particle mesh Ewald method.[16] A time step of 2 fs was used, and all of the bonds involving hydrogen atoms were constrained with the SHAKE method.[17] After an equilibration period with gradually released harmonic restraints, production simulations were performed at 310 K and 1 atm using Langevin temperature and Langevin piston pressure coupling schemes.[18,19] The TIP3P force field was used for water molecules,[20] and CHARMM force field was used for the protein and lipid atoms.[21] Simulations were performed with NAMD,[22] and continued for 200 ns for the 2+ state, and 300 ns for the 3+ state.

Quantum-Mechanical Optimization of the His37··· Trp41 Quartet Structure at 3+ State. To prepare the His37···Trp41 quartet structures for the subsequent H3- and D3-models at the acidic condition with QM/MM MD simulations, we followed the protocol used in our previous work[14,23] to optimize the His37···Trp41 quartet structure at the 2+ state with the ONIOM method[24] implemented in Gaussian 03.[25] On the basis of the optimized His37···Trp41 quartet structure in the H2- and D2-models, a third proton was added to a neutral His37 side chain, and ONIOM was used to optimize the system after this addition. Then, the H3 and D3-models were constructed with the original quartet in the corresponding H2(D2)-model replaced with the newly optimized quartet at the 3+ state. Therefore, the initial backbone of the H3(D3)-model is similar to the preceding H2(D2)-model. With the quartet structure held fixed, we then relaxed the remaining atoms of the H3(D3)-model with classical MD simulations for 20 ns. We took the last snapshot from the MD simulations, and minimized the system with the His37···Trp41 quartet fixed. The minimized structures were used for the following QM/MM MD simulations.
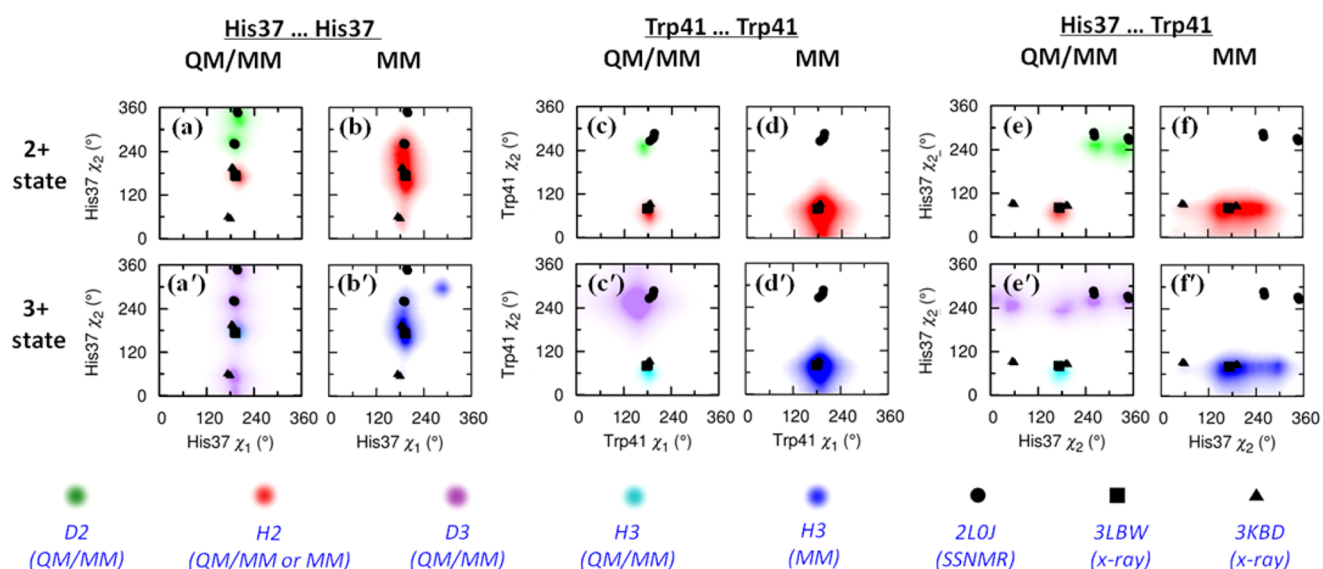
Figure 2. Dihedral angle distributions of the His37 and Trp41 side chains from the D- and H-models are plotted at neutral and acidic pH conditions. The top panel shows the plots at neutral conditions (2+ state), which are labeled as a−f; the corresponding plots at acidic conditions (3+ state) are labeled as a′−f′, shown in the bottom panel. The experimental structures at either condition are used for comparison. Panels a and b show the correlation between χ1 and χ2 on His37 side chain from the QM/MM and classical MD simulations, respectively. Panels c and d show the correlation between χ1 and χ2 on Trp41 side chains. Panels e and f show the correlation between χ2 on His37 and χ2 on Trp41.

QM/MM MD Simulations. In the QM/MM scheme, as in our previous study,[14] we included in the QM region the His37···Trp41 quartet and thirteen water molecules nearby (corresponding to the three water clusters identified in the 3LBW.pdb structure:[15] six waters just above the His37 tetrad, two in the His37···Trp41 cavity, and five below the Trp41 gate). These atoms were treated at the density functional theory (DFT) level using a mixed Gaussian and plane-waves treatment,[26] while the rest of the system, including the protein, the lipids, and waters, was treated with the MM method (CHARMM force field[21] and TIP3P[20]). The generalized gradient approximation (GGA) functional BLYP[27,28] with the D2 level dispersion-correction (BLYP-D2),[29] the triple-ζ basis set with two polarization functions,[30] and the Goedecker, Teter, and Hutter type pseudopotentials were used.[31] A wavelet-based Poisson solver was used to remove the spurious interactions of the QM region atoms with the periodic images.[32] A box size of $32 \times 32 \times 32$ Å^3 was used for the QM region so that the buffer between QM atoms and the box edge is ∼8 Å. We saturated the broken bonds with hydrogen atoms, and combined the QM and MM subsystems with the IMOMM methodology,[33] where the scaling factors of 1.355, 1.384, and 1.416 were used to relate the QM C−H bond distance to the MM Cα−C, Cα−N, and Cα−Cβ distances, respectively.

For the QM/MM MD simulations, after 2 ps equilibration for each model, we accumulated 9 ps trajectories for the D3-model with and without Cl$^-$, and 4 and 7 ps for H3-model with or without Cl$^-$, respectively.

To characterize the free energy profile for proton release from the His37 cluster in M2 protein, we followed the well-tested protocol used in the previous work from our group[34−36] to run constrained QM/MM MD simulations. The starting configuration was adopted from the preceding 3+ state QM/MM MD simulations. The reaction coordinate ζ was defined as the distance between the Nε2 on one His37 side chain and its neighboring Hε2, in the range of 1.0 Å to 1.6 Å. With the reaction coordinate ζ fixed in each window, constrained QM/MM MD simulations were carried out for times varying between 5 and 8 ps to obtain a converged PMF. Forces after the initial 1 ps of each constrained simulation were collected to calculate the mean constraint force. Free energy profiles for the proton release were estimated by thermodynamic integration of the mean force along the reaction coordinate.

All of the QM/MM MD simulations were carried out with the CP2K program[37] with a time step of 0.4 fs. The temperature was 310 K, using the Nose−Hoover chains thermostat[38] with a time constant of 1 fs.

Natural Bond Orbital (NBO) Analysis. NBO was used to calculate the partial charge at the MP2/6-311++G(d,p) level, performed with Gaussian 03.[25] In those calculations, only the side chains of the His37 and Trp41 residues were included, with the broken Cα-Cβ bonds saturated by hydrogen atoms.

■ RESULTS AND DISCUSSION

Structural Integrity. The conformation of the His37 cluster in both the D3-model and the H3-model was quantified by a single parameter, λ, defined as the projection of the atomic coordinates of His37 along the displacement vector connecting the two models, where λ = 0 represents the "dimer-of-dimers" (D2-model) and λ = 1 the "histidine-box" (H2-model).[14]

Upon binding the third proton, as shown in Figure 1D, the λ-value in the H3-model remains at ∼1, indicating that the protonation does not change the conformation of the His37 cluster significantly. In the D3-model, His37 shifts from λ = 0 to λ = 0.4, showing that the D2-model and the corresponding D3-model are connected by a pH-dependent transformation. Furthermore, this transformation appears to form an intermediate state of the one leading from the "dimer-of-dimers" (λ = 0) to the "histidine-box" (λ = 1). This conformational change has been previously proposed for the "dimer-of-dimers" at acidic conditions, where one dimer is broken upon taking a third proton, to avoid electrostatic repulsion.[23,39] The structure of the His37 cluster after this

conformational change is closer to the "histidine-box" conformation.

In both models, the presence of a Cl⁻ ion in the His37··· Trp41 cavity does not have a major impact on the protein's conformation (Figure 1B–D), but has more profound effects on proton conduction, which is further described below.

Rotamer Structures. *His37.* We monitored the specific structural motifs of either model by exploring the rotamer structures of His37 and Trp41. As disclosed by experimental determined structures at different conditions, these two key residues at both high and low pHs adopt rotameric angle χ_1 = 180°, whereas the angle χ_2 is relatively flexible.[15,39,40] In particular, the side chain dynamics of the two residues are distinct between the D- and the H-models.

In the QM/MM MD simulations at the 2+ state (Figure 2a), the His37 cluster in the D2-model adopts a 2-fold symmetry, where the two dihedral angles $[\chi_1, \chi_2]$ of the charged His37 side chains are $[180°, 360°]$ and those of the neutral ones are $[180°, 260°]$. The $[180°, 360°]$ configuration of His37 was rarely sampled in the classical MD simulations (Figure 2b and 2b′), largely because of the inability of the classical force field to reproduce the strongly hydrogen bonded "dimer-of-dimers" of the D2-model.[23,39] In the D3-model (Figure 2a′), one of the charged His37 side chain in the broken dimer remains at the $[180°, 60°]$ configuration with the other one swings at $[180°, 150° \sim 220°]$, and the intact histidine-pair resembles those in the D2-model. Interestingly, this $[180°, 60°]$ configuration is the characteristic of the low pH structure,[40] which was occasionally sampled in the classical MD simulations at the 2+ state, but never reached in the corresponding QM/MM MD simulations. In both the H2- and H3-models, all of the four His37 side chains have $[\chi_1, \chi_2]$ values of $[180°, 180°]$.

Trp41. The Trp41 side chains feature a "flip" variant in the H-models (the Nε1-Hε1 bond of the indole group points toward the central pore) and a "flop" variant in the D-models (the same bond points away from the central pore). These variants correspond to χ_2 angles located at ~80° (*tp* rotamer, the "flip" variant) and at ~280° (*tm* rotamer, the "flop" variant), which are retained at both high and low pH conditions in each model (Figure 2c and 2c′). However, the χ_2 angle of Trp41 at the low pH conditions in the D3-model is more diffuse than the congener in the D2-model, indicating a more dynamic Trp41 gate in the D-model under acidic conditions. In contrast, this gate seems to be more rigid in the H-models, as evidenced by the similar distributions of χ_2 angle at neutral or acidic pH conditions. Due to the inward orientation of Trp41 in the H3-model, the excess proton is less easy to be released toward the intraviral end of the channel, as further described below. However, this orientation enables the Trp41 side chains to form water-mediated hydrogen bonding interactions with Asp44 (Figure 3), which was proposed to stabilize the Trp41 gate, a critical factor for the asymmetric proton flux.[15,41] The outward orientation of the Trp41 in the D3-model, on the other hand, points the amide group toward the hydrophobic wall, which seems to be a less favorable factor for its gating.

It should be noted that, in the classical and QM/MM MD simulations of both D-models, only the *tp* rotamer of Trp41 was observed (Figure 2d and 2d′), as the "histidine-box" X-ray structure[15] was used as the initial structure and no indole ring flipping happened in the submicrosecond time scale simulations.

The average Hη2···Hη2 distance of neighboring Trp41 residues in the D2- and D3-models are 4.7 and 7.2 Å,
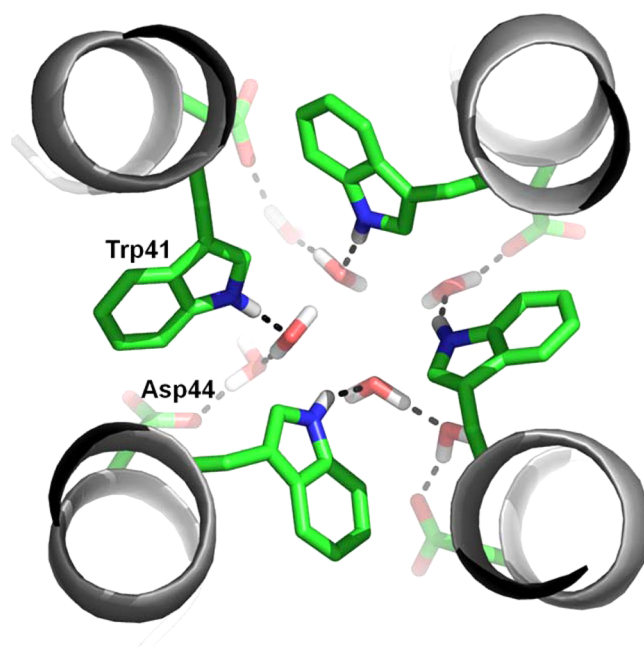

Figure 3. Interactions between Trp41 and Asp44 in the H3-model. Shown is the top view of the channel, in which Trp41, Asp44 and water molecules are the sticks, and the backbone of the protein is the spiral. His37 is omitted for clarity.

respectively, which are consistent with the data derived from ¹⁹F NMR measurement on ¹⁹F(HNM) M2TM sample (~3.2 Å at pH 8.0 and ~8.0 Å at pH 5.3).[42] In contrast, the average Hζ3···Hζ3 distance is ~11 Å in both the H2- and H3-models. This is in line with a NMR experiment under different conditions, in which the ¹⁹F(Hζ3) M2TM sample was found to have the closest distance of ~11 Å at both high and low pH conditions.[43]

His37···Trp41 Coupling. As the M2 protein's structure is sensitive to the change in the solubilizing environment,[1,44,45] the diversity of the His37···Trp41 contact depends on the balance between different rotamers. The nature of the interaction between His37 and Trp41 differs between the D- and H-models, as the former is more sensitive to the protonation state (Figure 2e,e′,f,f′). This difference in the His37···Trp41 packing and its response to the environment can be mainly attributed to the higher flexibility of the His37 side chain compared to Trp41. In the H-model, the orientations of the two residues and their coupling are less dependent on pH condition, showing only small thermal motions for both the imidazole ring of His37 and indole ring of Trp41.

Due to the different rotameric conformations, distances between His37 and Trp41 are also distinct in the D- and H-models, which can be determined by different techniques. As shown in Table 1, the distances measured in our MD simulations are quantitatively consistent with experimental structures or NMR measurements. Taking the Cδ(His37)··· Hζ3(Trp41) distance as an example, at neutral pH condition, the average distances (Figure 4a) in the D2- and H2-models are 6.8 and 4.7 Å, respectively, corresponding to 6.5 Å in the 2L0J.pdb[39] and 5.0 Å in the 3LBW.pdb.[15]

Free Energy Cost of Deprotonation. To explore the free energy cost for the His37 cluster to release a proton at low pH conditions, we carried out constrained QM/MM MD simulations on the D3- and H3-models imbedded in the fully hydrated lipid bilayers, in which the geometrical parameter of

12647

dx.doi.org/10.1021/jp5102225 | J. Phys. Chem. B 2014, 118, 12644−12651

Table 1. Geometric Parameters (in Å) of the His37···Trp41 Cluster in Different Computational Models and Experimental Structures

	D2	D3	H2	H3	2L0J[a,39]	3LBW[15]	3BKD[40]	SSNMR[c,54]
H(Nδ)···W(Cγ)	4.7	4.0	5.4	5.7	5.3[b]	5.5	4.2	/
H(Cγ)···W(Hζ3)	7.5	7.9	5.7	5.8	6.9	5.7	6.0	8.4[c] (6.2)
H(Cδ)···W(Hζ3)	6.8	7.3	4.7	4.8	6.5	5.0	7.0	/(6.0)
H(Cε)···W(Hζ3)	5.5	5.6	6.3	6.5	4.9	6.0	5.0	8.4 (7.3)
W(Hη3)···W(Hη3)	4.7	7.2	10.3	10.0	4.5	∼11	∼11	/
W(Hζ3)···W(Hζ3)	5.1	4	11.2	10.8	3.9	∼11	∼11	/

[a]Ensemble average of the eight snapshots of the NMR structure. [b]Among the eight snapshots of the NMR structures, the shortest is 4.4 Å. [c]Data at pH = 8.5 and pH = 4.5 (in parentheses) are shown. SSNMR: solid-state NMR.
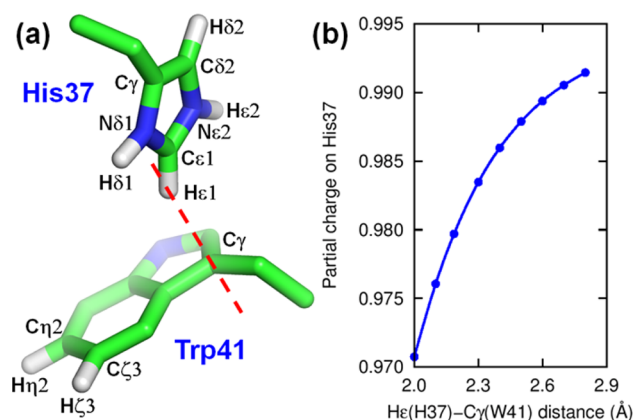

Figure 4. (a) Shown is the cation-π interaction between His37 and Trp41. The dashed line connecting Hε1 on His37 and Cγ on Trp41 indicates the reaction coordinate used to scan the change of partial charge, as shown in panel b. NBO analysis was used to calculate the partial charge at the MP2/6-311++G(d,p) level.

the distance between Nε2 on one His37 side chain and its neighboring Hε2 was selected as the reaction coordinate ζ. Among the three charged His37 residues, the one with the [χ1, χ2] of [180°, 60°] was selected to release a proton, as this His37 has an orientation similar to those found in the low pH condition X-ray structure.[40]

The free energy profiles for deprotonation and the representative snapshots along the reaction pathways are shown in Figure 5. The calculated PMFs was obtained by thermodynamic integration of the average force along the deprotonation pathway, where all free energy values are shown relative to the value of the lowest PMF calculated in each system (Figure 5a). The deprotonation curves are quite similar between the D3- and H3-models, but the presence of Cl$^-$ imposes significant perturbation on His37 deprotonation (describe later). In the D3-model, the minimum of the free energy profile is located at ζ = 1.024 Å, corresponding to the triply charged His37 cluster state (Figure 5a,b). Along with the increase of the Nε2−Hε2 bond until ζ = 1.30 Å, the PMF increases, showing that the proton moving from His37 to the neighboring water is energetically unfavorable (Figure 5a,b'). At ζ = 1.30 Å, the proton is shared by His37 and the neighboring water, with the average Nε2(His37)···O(water) distance of 2.52 Å, where the proton is closer to the water (the averaged Hε2···O(water) distance is 1.24 Å). The newly formed hydronium is stabilized by the surrounding hydrogen-bond network, which extends to the waters at the C-terminal side (Figure 5b''). At high pH conditions, these interactions are interrupted as the Trp41 gate is closed. Meanwhile, one proton of the hydronium points to the neighboring water, and is ready

to be released. Beyond this point, the PMF decreases. The barrier height for proton release is 6.35 kcal/mol. The additional proton on the hydronium is expected to release to the C-terminal side of the pore. At ζ = 1.5 Å, the proton transfer is complete (the averaged Hε2···O(water) distance is 1.06 Å), and the hydronium group is separated from His37 by three water molecules. The mechanism of proton release in the H3-model (Figure 5a,c−c'') is very similar to that in the D3-model, with the free energy barrier height of 6.63 kcal/mol, located at ζ = 1.36 Å: at this point, a hydronium is formed next to the deprotonated His37 (with the Nε2(His37)···O(water) and Hε2···O(water) distances of 2.53 and 1.22 Å, respectively).

Previously, we demonstrated that two alternative configurations (the D2- and H2-models) are capable of stabilizing the charges in the pore at neutral pH condition.[14] Here we find that, under acidic conditions, the mechanism of proton release from the His37 cluster is much less dependent on its configuration (the D3- or H3-models). In other words, for a charged His37 side chain, which is ready to lose a proton, it is largely unaffected by the configuration of the remaining three His37 residues. Therefore, the interplay between His37 residues, the pH sensor of the channel, is pH dependent during the proton relay. The Trp41 gate and the membrane environment, on the other hand, are likely to play a role in modulating the rate of deprotonation and thus the conductance.

Different computational approaches have previously been used to explore the deprotonation from the charged His37 cluster in the M2 protein.[34−36,46] In one recent paper from our group, the deprotonation from a single histidine and from the His···Trp motif in water was investigated with DFT-based MD simulations.[34] For a single histidine, the free energy barriers were calculated to be 10.0−10.1 kcal/mol at the Nδ position, and 10.5−10.6 kcal/mol at the Nε position. A recent study from Voth and co-workers combined an empirical valence bond and a DFT-based QM/MM approach to study the proton release at different protonation states, reporting barrier heights of ∼13 and ∼10 kcal/mol for proton release from the triply and quadruply charged His37 cluster, respectively.[46]

When a single Trp residue is included in the calculation with a position resembling that in the protein, the barrier for the Nδ was found to be 9.1 kcal/mol, ∼1 kcal/mol lower than that in the isolated histidine in water box,[34] suggesting a role of the Trp41 gate in regulating the proton relay through His37, in addition to its known ability to generate an asymmetric flow.[15] Specifically, charge transfer from His37 to the bound Trp41 through the cation−π interactions was witnessed, as assessed by the partial charge on each group (Figure 4b), consistently with the calculated electrostatic potential.[23] Presumably, this charge delocalization decreases the energy cost to lose a proton.
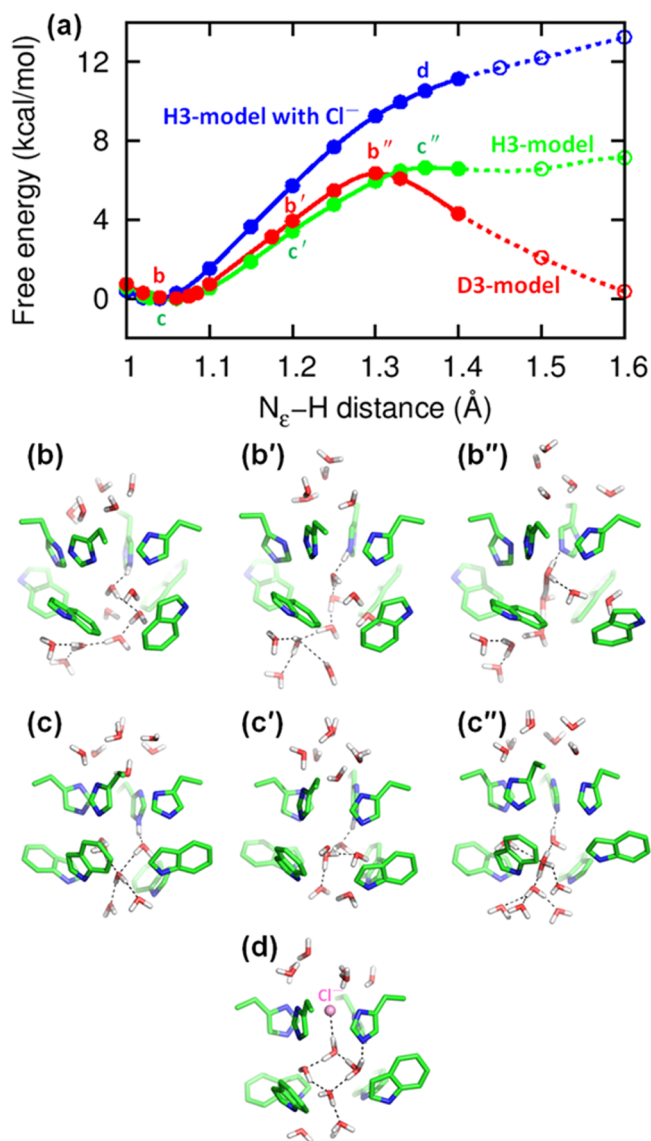
Figure 5. (a) Shown are the free energy profiles for proton release under different starting configurations. Both the D3- and H3-models have similar deprotonation pathways, while the presence of Cl⁻ in the H3-model inhibits proton release. Panels b−d show the representative snapshots during the proton release in the D3-model (b−b″), the H3-model (c−c″), and the H3-model with Cl⁻ (d). Their locations are labeled in panel a. Taking the D3-model as an example, along its deprotonation pathway, one proton originally attached to the Nε on a charged His37 residue gradually moved to the neighboring water cluster at the C-terminal side, with the Nε−H distance increased from 1.024 Å (b) to 1.20 Å (b′) and to 1.30 Å (b″). At 1.30 Å, the proton is shared by His37 and the water cluster. Further increase of the Nε−H distance enables the fully release of the proton from His37, as shown on the red dashed line in (a).

In the present work, the energy cost for deprotonation in the membrane environment is ∼6.5 kcal/mol, significantly lower than the one in the His···Trp motif or the isolated His.[34] Apparently, the present work provides a more realistic model in studying proton transfer, where the backbone of the trans-membrane domain of the protein, the Trp41 gate, and the explicit membrane environment have significant effects on modulating the dissociation of protons from His37. For the latter one, to be specific, the confined environment of the pore and the low dielectric constant of the membrane destabilize the

charged cluster, and thus facilitate the deprotonation of the charged His37. By using the following equations and assuming $\Delta G = 0$ for simplicity between His37 and bulk water,[36] the upper limit of the pK_a of His37 in the membrane environment is estimated to be 4.7 in the D3-model and 5.0 in the H3-model, respectively, based on the major barrier heights for deprotonation in both models. Experimentally, the third pK_a of the His37 cluster—when three of four residues are protonated—was determined as 6.3[47] and 4.9 ± 0.3,[48] respectively, by using different protein constructs and lipid membrane compositions.

$$\Delta G = \Delta G^0 + 2.303 RT \log\left(\frac{[\text{His}][\text{H}^+]}{[\text{HisH}^+]}\right)$$

$$\Delta G^0 = 2.303 RT \, \text{p} K_a$$

The backbone conformations in both D3- and H3-models are very similar to those of the relatively compact protein structure at neutral pH.[15] Without significant expansion of the backbone, we demonstrate that both models are able to release a proton with a moderate energy cost. The presence of the C-terminal amphipathic helix anchoring at the lipid interfacial region is likely to limit the dynamic of the C-terminal segment,[39] compared to what seen for the isolated the transmembrane helices from electron paramagnetic resonance (EPR) experiments[49,50] and the X-ray structure determined at low pH conditions.[40]

Role of Anion in the Pore. Finally, we investigated the possibility of a role for Cl⁻ or other halide anions in the proton relay mechanism through the pore. In electrophysiology studies, the proton conduction rate was found to be unaffected by the concentration of Cl⁻ in both oocytes[40,41] and liposomes.[51] This finding is in apparent contrast with the attractive force that a triply charged His37 tetrad can exert on a Cl⁻ ion:[52] assuming for simplicity that the rate of proton transfer is only controlled by electrostatics, Cl⁻ ions should increase the proton conduction rate. In a recent study of the calcium-release activated calcium channel (CRAC), a cation-conducing channel with a 6 Å-wide pore and a high density of basic side chains, we observed that Cl⁻ anions in the pore significantly increase the rate of permeation of Na⁺ cations.[53] Therefore, we extended the proton transfer calculations to a model including a Cl⁻ ion bound to the His37 tetrad, to explore its impact on the proton conduction rate.

As shown in the PMF calculations, the presence of Cl⁻ makes the free energy cost of deprotonation much higher. Following the increasing N−H distance, the PMF keeps rising: at ζ =1.36 Å, where the major barrier is located in the previous PMFs, the free energy value is 10.5 kcal/mol, 3.9 kcal/mol higher than that in the H3-model (Figure 5a). This demonstrates that the presence of Cl⁻ creates an unfavorable pathway for a proton to be released. During the simulations, the Cl⁻ ion is located in the highly charged His37 cluster, and has stable interactions with the water in the cavity below, which is formed by the His37 and Trp41 clusters (Figure 5d). The arrangement of the hydrogen bonding network of water molecules in the cavity could compensate in principle the energy cost for bond breaking of the proton release. Nevertheless, the electrostatic attraction between the anion and the proton attenuates the proton diffusion out of the cavity to the C-terminal even though the Trp41 gate is occasionally open. Therefore, the presence of anions in the His37···Trp41

cavity is an unfavorable factor for proton release, which the M2 channel can circumvent by maintaining its pore free of Cl^- ions through its Asp44 residues, two helical turns away from His37. This is confirmed by mutations of Asp44, which significantly impact the proton conduction profile in a salt solution with a $[Cl^-]/[SO_4^{2-}]$ ratio approximately 2:1.[41]

■ CONCLUSIONS

In this study, we explored the different configurations of the His37···Trp41 cluster in the M2 protein at low pH conditions, and the subsequent deprotonation via QM/MM MD simulations. With regard to the conformation of the key residues, two alternative models (D3 and H3) converge to a single deprotonation mechanism, and feature similar free energy profiles to release a proton, with a barrier height of ~6.5 kcal/mol. Therefore, the multiconfiguration model proposed in our previous work,[14] includes deprotonation as a mechanism not only for proton conduction, but also for conformational exchange connecting the multiple configurations of this protein. The confined region between His37 and Trp41 also appears to significantly increase the proton affinity of a water molecule compared to the bulk solution. Calculations with a bound Cl^- ion in the pore show that halide anions may contribute to stabilizing the triply charged histidine cluster, but at the same time impede the release of protons. We suggest that only those viral strains capable of maintaining halide anions outside the pore can maintain a stable proton conduction rate irrespective of the anions' bulk concentration.

■ AUTHOR INFORMATION

Corresponding Author

*E-mail: mike.klein@temple.edu.

Notes

The authors declare no competing financial interest.

■ ACKNOWLEDGMENTS

■ REFERENCES

(1) Cross, T. A.; Dong, H.; Sharma, M.; Busath, D. D.; Zhou, H.-X. M2 Protein from Influenza A: From Multiple Structures to Biophysical and Functional Insights. *Curr. Opin. Virol.* **2012**, *2*, 128−133.

(2) Pinto, L. H.; Lamb, R. A. The M2 Proton Channels of Influenza A and B Viruses. *J. Biol. Chem.* **2006**, *281*, 8997−9000.

(3) Mould, J. A.; Li, H. C.; Dudlak, C. S.; Lear, J. D.; Pekosz, A.; Lamb, R. A.; Pinto, L. H. Mechanism for Proton Conduction of the M2 Ion Channel of Influenza A Virus. *J. Biol. Chem.* **2000**, *275*, 8592−8599.

(4) Mould, J. A.; Drury, J. E.; Frings, S. M.; Kaupp, U. B.; Pekosz, A.; Lamb, R. A.; Pinto, L. H. Permeation and Activation of the M2 Ion Channel of Influenza A Virus. *J. Biol. Chem.* **2000**, *275*, 31038−31050.

(5) Chizhmakov, I. V.; Geraghty, F. M.; Ogden, D. C.; Hayhurst, A.; Antoniou, M.; Hay, A. J. Selective Proton Permeability and pH Regulation of the Influenza Virus M2 Channel Expressed in Mouse Erythroleukaemia Cells. *J. Physiol. London* **1996**, *494*, 329−336.

(6) Venkataraman, P.; Lamb, R. A.; Pinto, L. H. Chemical Rescue of Histidine Selectivity Filter Mutants of the M2 Ion Channel of Influenza A Virus. *J. Biol. Chem.* **2005**, *280*, 21463−21472.

(7) Wang, C.; Lamb, R. A.; Pinto, L. H. Activation of the M2 Ion Channel of Influenza Virus: A Role for the Transmembrane Domain Histidine Residue. *Biophys. J.* **1995**, *69*, 1363−1371.

(8) Poishchuk, A. L.; Cristian, L.; Pinto, L. H.; Lear, J. D.; DeGrado, W. F. Mechanistic Insights from Functional Characterization of an Unnatural His37 Mutant of the Influenza A/M2 Protein. *Biochim. Biophys. Acta, Biomembr.* **2014**, *1838*, 1082−1087.

(9) Hong, M.; Degrado, W. F. Structural Basis for Proton Conduction and Inhibition by the Influenza M2 Protein. *Protein Sci.* **2012**, *21*, 1620−1633.

(10) Tang, Y. J.; Zaitseva, F.; Lamb, R. A.; Pinto, L. H. The Gate of the Influenza Virus M_2 Proton Channel Is Formed by a Single Tryptophan Residue. *J. Biol. Chem.* **2002**, *277*, 39880−39886.

(11) Okada, A.; Miura, T.; Takeuchi, H. Protonation of Histidine and Histidine-Tryptophan Interaction in the Activation of the M2 Ion Channel from Influenza A Virus. *Biochemistry* **2001**, *40*, 6053−6060.

(12) Zhou, H.-X.; Cross, T. A. Modeling the Membrane Environment Has Implications for Membrane Protein Structure and Function: Influenza A M2 Protein. *Protein Sci.* **2013**, *22*, 381−394.

(13) Carnevale, V.; Fiorin, G.; Levine, B. G.; DeGrado, W. F.; Klein, M. L. Multiple Proton Confinement in the M2 Channel from the Influenza A Virus. *J. Phys. Chem. C* **2010**, *114*, 20856−20863.

(14) Dong, H.; Fiorin, G.; Degrado, W. F.; Klein, M. L. Exploring Histidine Conformations in the M2 Channel Lumen of the Influenza A Virus at Neutral pH via Molecular Simulations. *J. Phys. Chem. Lett.* **2013**, *4*, 3067−3071.

(15) Acharya, R.; Carnevale, V.; Fiorin, G.; Levine, B. G.; Polishchuk, A. L.; Balannik, V.; Samish, I.; Lamb, R. A.; Pinto, L. H.; DeGrado, W. F.; Klein, M. L. Structure and Mechanism of Proton Transport through the Transmembrane Tetrameric M2 Protein Bundle of the Influenza A Virus. *Proc. Natl. Acad. Sci. U.S.A.* **2010**, *107*, 15075−15080.

(16) Essmann, U.; Perera, L.; Berkowitz, M. L.; Darden, T.; Lee, H.; Pedersen, L. G. A Smooth Particle Mesh Ewald Method. *J. Chem. Phys.* **1995**, *103*, 8577−8593.

(17) Ryckaert, J. P.; Ciccotti, G.; Berendsen, H. J. C. Numerical Integration of Cartesian Equations of Motion of a System with Constraints: Molecular Dynamics of N-Alkanes. *J. Comput. Phys.* **1977**, *23*, 327−341.

(18) Feller, S. E.; Zhang, Y. H.; Pastor, R. W.; Brooks, B. R. Constant Pressure Molecular Dynamics Simulation: The Langevin Piston Method. *J. Chem. Phys.* **1995**, *103*, 4613−4621.

(19) Martyna, G. J.; Tobias, D. J.; Klein, M. L. Constant Pressure Molecular Dynamics Algorithms. *J. Chem. Phys.* **1994**, *101*, 4177−4189.

(20) Jorgensen, W. L.; Chandrasekhar, J.; Madura, J. D.; Impey, R. W.; Klein, M. L. Comparison of Simple Potential Functions for Simulating Liquid Water. *J. Chem. Phys.* **1983**, *79*, 926−935.

(21) MacKerell, A. D., Jr.; Banavali, N.; Foloppe, N. Development and Current Status of the CHARMM Force Field for Nucleic Acids. *Biopolymers* **2000**, *56*, 257−65.

(22) Phillips, J. C.; Braun, R.; Wang, W.; Gumbart, J.; Tajkhorshid, E.; Villa, E.; Chipot, C.; Skeel, R. D.; Kale, L.; Schulten, K. Scalable Molecular Dynamics with NAMD. *J. Comput. Chem.* **2005**, *26*, 1781−1802.

(23) Dong, H.; Yi, M.; Cross, T. A.; Zhou, H.-X. *Ab Initio* Calculations and Validation of the pH-Dependent Structures of the His37-Trp41 Quartet, the Heart of Acid Activation and Proton Conductance in the M2 Protein of Influenza A Virus. *Chem. Sci.* **2013**, *4*, 2776−2787.

(24) Svensson, M.; Humbel, S.; Froese, R. D. J.; Matsubara, T.; Sieber, S.; Morokuma, K. ONIOM: A Multilayered Integrated MO +MM Method for Geometry Optimizations and Single Point Energy Predictions. A Test for Diels-Alder Reactions and Pt(P(*t*-Bu)$_3$)$_2$+H$_2$ Oxidative Addition. *J. Phys. Chem.* **1996**, *100*, 19357−19363.

12650

dx.doi.org/10.1021/jp5102225 | *J. Phys. Chem. B* 2014, 118, 12644−12651

(25) Frisch, M. J.; Trucks, G. W.; Schlegel, H. B.; Scuseria, G. E.; Robb, M. A.; Cheeseman, J. R.; Montgomery, J. A.; Vreven, T.; Kudin, K. N.; Burant, J. C., et al. *Gaussian 03*, revision E.01; Gaussian, Inc.: Wallingford, CT, 2004.

(26) Lippert, G.; Hutter, J.; Parrinello, M. A. Hybrid Gaussian and Plane Wave Density Functional Scheme. *Mol. Phys.* **1997**, *92*, 477−487.

(27) Lee, C. T.; Yang, W. T.; Parr, R. G. Development of the Colle−Salvetti Correlation-Energy Formula into a Functional of the Electron Density. *Phys. Rev. B* **1988**, *37*, 785−789.

(28) Becke, A. D. Density-Functional Exchange-Energy Approximation with Correct Asymptotic Behavior. *Phys. Rev. A* **1988**, *38*, 3098−3100.

(29) Grimme, S. Semiempirical Hybrid Density Functional with Perturbative Second-Order Correlation. *J. Chem. Phys.* **2006**, *124*, 034108.

(30) VandeVondele, J.; Hutter, J. Gaussian Basis Sets for Accurate Calculations on Molecular Systems in Gas and Condensed Phases. *J. Chem. Phys.* **2007**, *127*, 114105.

(31) Goedecker, S.; Teter, M.; Hutter, J. Separable Dual-Space Gaussian Pseudopotentials. *Phys. Rev. B* **1996**, *54*, 1703−1710.

(32) Genovese, L.; Deutsch, T.; Goedecker, S. Efficient and Accurate Three-Dimensional Poisson Solver for Surface Problems. *J. Chem. Phys.* **2007**, *127*, 054704.

(33) Maseras, F.; Morokuma, K. Imomm: A New Integrated *Ab Initio* + Molecular Mechanics Geometry Optimization Scheme of Equilibrium Structures and Transition-States. *J. Comput. Chem.* **1995**, *16*, 1170−1179.

(34) Bankura, A.; Klein, M. L.; Carnevale, V. Proton Affinity of the Histidine-Tryptophan Cluster Motif from the Influenza A Virus from *Ab Initio* Molecular Dynamics. *Chem. Phys.* **2013**, *422*, 156−164.

(35) Ivanov, I.; Chen, B.; Raugei, S.; Klein, M. L. Relative pK_a Values from First-Principles Molecular Dynamics: The Case of Histidine Deprotonation. *J. Phys. Chem. B* **2006**, *110*, 6365−6371.

(36) Ivanov, I.; Klein, M. L. Deprotonation of a Histidine Residue in Aqueous Solution using Constrained *Ab Initio* Molecular Dynamics. *J. Am. Chem. Soc.* **2002**, *124*, 13380−13381.

(37) VandeVondele, J.; Krack, M.; Mohamed, F.; Parrinello, M.; Chassaing, T.; Hutter, J. QUICKSTEP: Fast and Accurate Density Functional Calculations Using a Mixed Gaussian and Plane Waves Approach. *Comput. Phys. Commun.* **2005**, *167*, 103−128.

(38) Martyna, G. J.; Klein, M. L.; Tuckerman, M. Nose-Hoover Chains: The Canonical Ensemble via Continuous Dynamics. *J. Chem. Phys.* **1992**, *97*, 2635−2643.

(39) Sharma, M.; Yi, M. G.; Dong, H.; Qin, H. J.; Peterson, E.; Busath, D. D.; Zhou, H.-X.; Cross, T. A. Insight into the Mechanism of the Influenza A Proton Channel from a Structure in a Lipid Bilayer. *Science* **2010**, *330*, 509−512.

(40) Stouffer, A. L.; Acharya, R.; Salom, D.; Levine, A. S.; Di Costanzo, L.; Soto, C. S.; Tereshko, V.; Nanda, V.; Stayrook, S.; DeGrado, W. F. Structural Basis for the Function and Inhibition of an Influenza Virus Proton Channel. *Nature* **2008**, *451*, 596−599.

(41) Ma, C.; Fiorin, G.; Carnevale, V.; Wang, J.; Lamb, R. A.; Klein, M. L.; Wu, Y.; Pinto, L. H.; DeGrado, W. F. Asp44 Stabilizes the Trp41 Gate of the M2 Proton Channel of Influenza A Virus. *Structure* **2013**, *21*, 2033−2041.

(42) Witter, R.; Nozirov, F.; Sternberg, U.; Cross, T. A.; Ulrich, A. S.; Fu, R. Solid-State ^{19}F NMR Spectroscopy Reveals that Trp_{41} Participates in the Gating Mechanism of the M2 Proton Channel of Influenza A Virus. *J. Am. Chem. Soc.* **2008**, *130*, 918−924.

(43) Luo, W.; Mani, R.; Hong, M. Side-Chain Conformation of the M2 Transmembrane Peptide Proton Channel of Influenza A Virus from ^{19}F Solid-State NMR. *J. Phys. Chem. B* **2007**, *111*, 10825−10832.

(44) Claridge, J. K.; Aittoniemi, J.; Cooper, D. M.; Schnell, J. R. Isotropic Bicelles Stabilize the Juxtamembrane Region of the Influenza M2 Protein for Solution NMR Studies. *Biochemistry* **2013**, *52*, 8420−8429.

(45) Cross, T. A.; Sharma, M.; Yi, M.; Zhou, H.-X. Influence of Solubilizing Environments on Membrane Protein Structures. *Trends Biochem. Sci.* **2011**, *36*, 117−125.

(46) Liang, R.; Li, H.; Swanson, J. M.; Voth, G. A. Multiscale Simulation Reveals a Multifaceted Mechanism of Proton Permeation through the Influenza A M2 Proton Channel. *Proc. Natl. Acad. Sci. U.S.A.* **2014**, *111*, 9396−9401.

(47) Hu, J.; Fu, R.; Nishimura, K.; Zhang, L.; Zhou, H.-X.; Busath, D. D.; Vijayvergiya, V.; Cross, T. A. Histidines, Heart of the Hydrogen Ion Channel from Influenza A Virus: Toward an Understanding of Conductance and Proton Selectivity. *Proc. Natl. Acad. Sci. U.S.A.* **2006**, *103*, 6865−6870.

(48) Hu, F.; Schmidt-Rohr, K.; Hong, M. NMR Detection of pH-Dependent Histidine-Water Proton Exchange Reveals the Conduction Mechanism of a Transmembrane Proton Channel. *J. Am. Chem. Soc.* **2012**, *134*, 3703−3713.

(49) Thomaston, J. L.; Nguyen, P. A.; Brown, E. C.; Upshur, M. A.; Wang, J.; DeGrado, W. F.; Howard, K. P. Detection of Drug-Induced Conformational Change of a Transmembrane Protein in Lipid Bilayers Using Site-Directed Spin Labeling. *Protein Sci.* **2013**, *22*, 65−73.

(50) Nguyen, P. A.; Soto, C. S.; Polishchuk, A.; Caputo, G. A.; Tatko, C. D.; Ma, C. L.; Ohigashi, Y.; Pinto, L. H.; DeGrado, W. F.; Howard, K. P. pH-Induced Conformational Change of the Influenza M2 Protein C-Terminal Domain. *Biochemistry* **2008**, *47*, 9934−9936.

(51) Leiding, T.; Wang, J.; Martinsson, J.; DeGrado, W. F.; Arskold, S. P. Proton and Cation Transport Activity of the M2 Proton Channel from Influenza A Virus. *Proc. Natl. Acad. Sci. U.S.A.* **2010**, *107*, 15409−15414.

(52) Wei, C.; Pohorille, A. Activation and Proton Transport Mechanism in Influenza A M2 Channel. *Biophys. J.* **2013**, *105*, 2036−2045.

(53) Dong, H.; Klein, M. L.; Fiorin, G. Counterion-Assisted Cation Transport in a Biological Calcium Channel. *J. Phys. Chem. B* **2014**, *118*, 9668−9676.

(54) Williams, J. K.; Zhang, Y.; Schmidt-Rohr, K.; Hong, M. pH-Dependent Conformation, Dynamics, and Aromatic Interaction of the Gating Tryptophan Residue of the Influenza M2 Proton Channel from Solid-State NMR. *Biophys. J.* **2013**, *104*, 1698−1708.